Title

A Test of Geophysical Prospecting for the Detection of Prehistoric Canals on the Gila River Reservation, Arizona

Authors

Hildebrand, John

Wiggins, Sean

Henkart, Paul

et al.

Publication Date

2011-02-01

Report to the Gila River Indian Community

A Test of Geophysical Prospecting for the Detection of Prehistoric Canals on the Gila River Reservation, Arizona

John A. Hildebrand[1], Sean M. Wiggins[1], Paul Henkart[1], and Larry Conyers[2]

[1]Scripps Institution of Oceanography, University of California San Diego, La Jolla, CA 92093 USA
[2]Department of Anthropology, Denver University, Denver, CO 80208 USA

MPL TM- 531
February 2011

Executive Summary

This report documents a project to apply geophysical prospecting techniques at known locations of prehistoric canals in the Gila River Reservation. The project goal was to test the ability of several geophysical prospecting techniques to image buried canals in the Gila River floodplain.

Four geophysical prospecting approaches were tested: ground penetrating radar, seismic reflection imaging, magnet gradiometry, and electrical conductivity. These approaches have complimentary abilities to reveal buried objects and structures. Ground penetrating radar transmits high frequency electromagnetic energy into the ground and measures energy reflected from buried interfaces, such as between sand and other soil layers. Seismic reflection imaging similarly looks at reflected energy, but uses seismic waves as an energy source. Magnetometry is sensitive to the magnetic field that is emitted by buried objects and structures; it is particularly sensitive to the presence of burned objects, as well as to the sedimentary fill of a canal. Electrical conductivity uses low frequency electromagnetic energy to detect changes in electrical properties; it is an effective means for detecting soil moisture content changes, such as may be present in a buried canal.

Three sites with known prehistoric canals were investigated: GR-441 (Santan Site), GR-1086 (Crown Site), and GR-415. At each site, a prehistoric canal had previously been discovered by excavation. Geophysical prospecting data were collected adjacent to known canal locations so that the ability of each geophysical technique could be tested.

Ground penetrating radar had little or no penetration of site soils. It is likely that the high salt content of the Gila River floodplain yielded high attenuation of the 400 Mhz radar signals.

Using high-frequency seismic sources produced seismic reflection images with indications of the presence of a prehistoric canal. Seismic images revealed coherent reflections from the sloping sides and bottom of the canal features. These data are interpreted as owing to the contrast between sandy fill and clay layers forming the sides and bottom of the canal.

Electrical Conductivity data reveal broad regions of conductivity that follow the general trends of the canals. At each of these sites, regions of high and low conductivity are delimited by the location of the canal.

Magnetometry data collected at these sites was largely contaminated by the presence of modern metal fragments. The signal from these strongly magnetic objects located at or near the site surface made it difficult to discern if a low level signal was present owing to the buried prehistoric canal.

Introduction

Although prehistoric canals have previously been studied with geophysical methods (Jones et al. 2000; Karastathis et al. 2001), prehistoric canals of the US Southwest have not been previously investigated with geophysical methods. The Southwest environment presents significant challenges for geophysical methods owing to the arid soils and potentially high salt content.

Geological and Archaeological Setting

The Gila River is a tributary of the Colorado River, stretching across central Arizona. The middle Gila River is the location of the Gila River Reservation; it has a wide streambed with braided bars and channels composed of sand and gravel. The Gila River streambed is flanked by multiple active floodplain levels (T-0) and three terraces (T-1, T-2, T-3; see Waters et al. 2000).

Three sites were selected for study (GR-441, GR-1086, and GR-415) based on known locations for prehistoric canals (Figure 1). Two of these sites (GR-1086 and GR415) are located on terrace T-2, and one site (GR-441) is located on the adjacent alluvial piedmont of the Santan Mountains. These canals were part of a prehistoric network of canals constructed by the Hohokam to transport water for irrigation. The canals are larger at their junction with the Gila River, and become reduced in size away from the river. At the three sites investigated in this report, the canals have cross-sections that are several meters wide and 1-2 meters deep.

Geophysical Methods

Four geophysical techniques for site characterization were tested at the Gila River sites: Ground Penetrating Radar (GPR), ultra-shallow Seismic Reflection Imaging (SRI), Magnetic gradiometry (MAG), and ElectroMagnetic induction (EM). The goal of this work was to test if the Gila River site canals can be detected by geophysical methods.

Ground Penetrating Radar

The GPR method involves the transmission of high frequency electromagnetic radio (radar) pulses into the earth and measuring the time elapsed between transmission, reflection off a buried discontinuity and reception back at a surface radar antenna. A pulse of radar energy is generated on a transmitting antenna that is placed on, or near, the ground surface. The resulting wave of electromagnetic energy propagates into the ground where some energy can be reflected back to the surface by buried discontinuities. The discontinuities where reflections occur are usually created by changes in electrical properties of the sediment or soil, lithologic changes, differences in bulk density at stratigraphic interfaces and most important water content variations. Reflection can also occur at interfaces between anomalous archaeological features and the surrounding soil or sediment. As radar pulses are being transmitted through various materials on their way to the buried target feature, the velocity of propagation may change, depending on the physical and chemical properties of the material through which they are traveling. When the travel times of the energy pulses are measured

and their velocity through the ground is known (Conyers and Lucius, 1995), distance (or depth in the ground) can be accurately measured, producing a three-dimensional image of the subsurface.

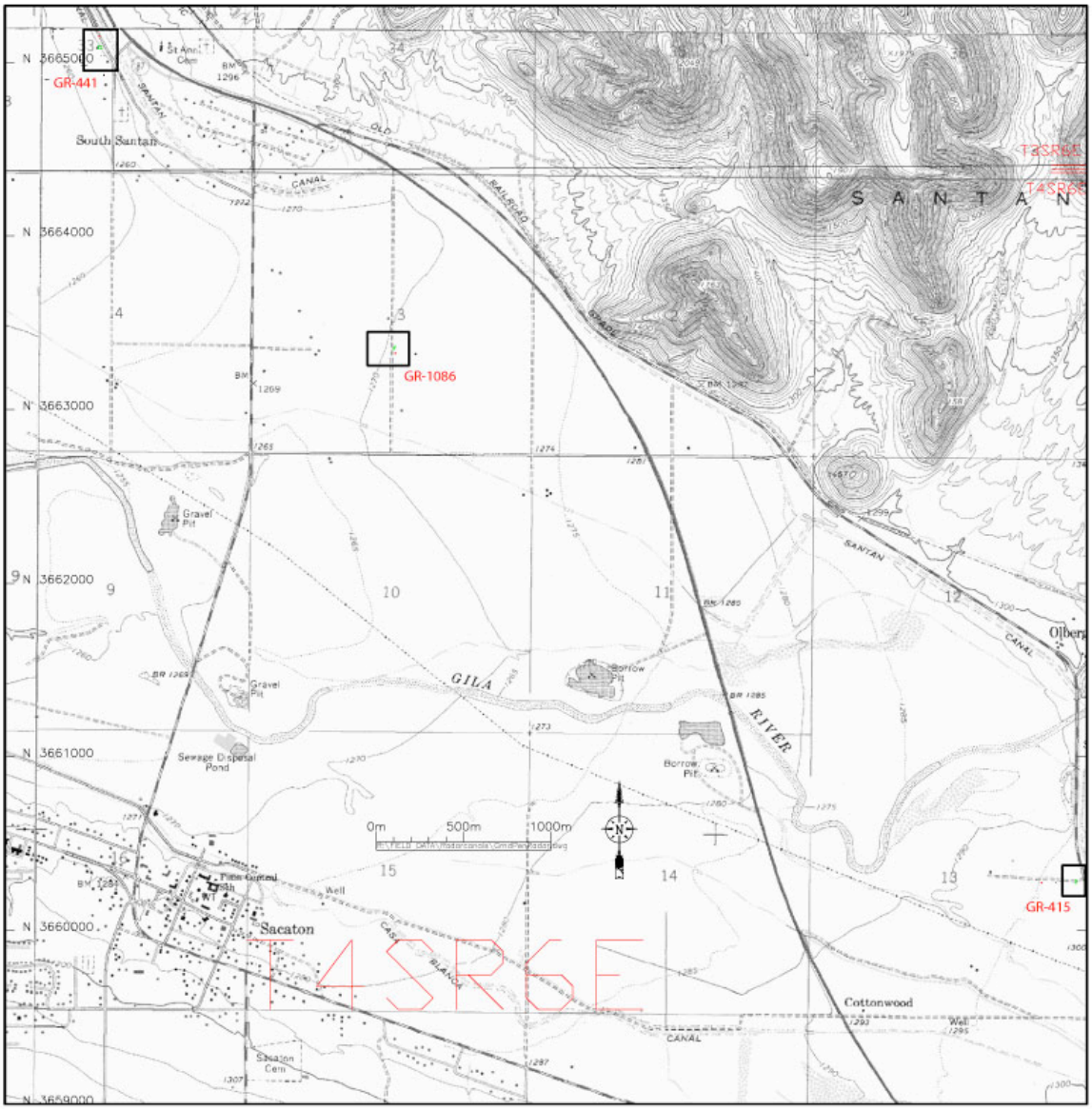

Figure 1. Location of Geophysical testing along the middle Gila River in Arizona. Areas of investigation are designated by boxes with red label for site number.

Typically GPR radar antennas are moved along the ground in transects and two-dimensional profiles of a large number of reflections at various depths are created, producing profiles of subsurface stratigraphy and buried archaeological features along lines. When data are acquired in a closely-spaced series of transects within a grid, and reflections are correlated and processed, an accurate three-dimensional picture of buried features and associated

stratigraphy can be constructed (Conyers 2004). This can be done visually by analyzing each profile, or with the aid of computer software that creates maps of many thousands of reflection amplitudes from all profiles in a grid. Ground-penetrating radar surveys allow for relatively wide aerial coverage in a short period of time, with excellent subsurface resolution. This three-dimensional resolution often gives GPR an advantage over other near-surface methods with respect to buried archaeological feature resolution.

The success of GPR surveys is to a great extent dependent on soil and sediment mineralogy, clay content, ground moisture, depth of burial, surface topography and vegetation (Conyers 2004). In the Gila River area the high clay and salt content in the alluvium attenuated radar energy within about 40 cm of the ground surface. The depth to which radar energy can penetrate and the amount of definition that can be expected in the subsurface is partially controlled by the frequency of the radar energy transmitted. Radar energy frequency controls both the wavelength of the propagating wave and the attenuation of the waves in the ground. Antennas usually come in standard frequencies, with each antenna having one center-frequency, but actually producing radar energy that ranges around that center by about two octaves (one half and two times the center frequency). In the Gila River surveys we used the 500 and 300 MHz antennas (GSSI SIR 2000). Both were capable of only about 40 cm depth penetration, or about 10 nanoseconds or less.

The Gila River site soils proved to be highly attenuative of GPR signals probably due to the prominence of salt. Despite significant effort no usable GPR data were collected at the Gila River sites due to lack of signal penetration of the radar (~ 40 cm).

Ultra-shallow seismic reflection

Seismic reflection imaging uses sources and receivers of elastic energy at the surface of the earth to detect buried layers or objects. Energy transmitted into the ground is returned to the surface by reflection from changes in material impedance (density and velocity). Seismic waves propagate in three modes: primary waves (P), shear waves (S), and surface or interface waves.

The resolving power for seismic reflection imaging is limited by the wavelength of the energy source and by the frequency response of the sensors. High frequencies (small wavelengths) are needed to resolve closely spaced features. Likewise, horizontal resolution is determined by source wavelength and receiver spacing. Attenuation and scattering increase for short wavelengths, placing practical limits on the frequency and therefore the overall imaging resolution.

Typical P-wave velocities range between 50 and 250m/s for dry unconsolidated soils and sediments. Shear wave velocities are typically less than 1/2 those of P-waves. Wavelengths for P-waves may be as small as 0.10m for high frequencies in soil (1000 Hz and 100m/s).

The geometry for seismic reflection locates sources and receivers at the ground surface. The source energy comes from a hammer strike or other impulse at the ground surface. Geophones may be 'planted' into the ground with a bottom-mounted spike pressed into the soil or contained in a bag of soil that is dragged along the ground surface (Steeples *et al.* 1999, Hildebrand *et al*. 2007). The reflected energy is received by geophones at multiple locations along the ground surface. Reflected energy time-series are converted to depth using knowledge of the propagation velocity.

To minimize the time and labor required for shallow seismic reflection imaging surveys, we modified a conventional system to allow for rapid movement of the sensors, source and recording system. The primary modification was to remove the planting spikes from the geophones (Mark Products L-14) and mount them on a thin flexible plastic board in a bag of wet sand. An array of 24 geophones was used, with sensors separations of 0.05m. Two sources were used: (1) a 0.30m long by 0.025m diameter pipe held vertically on the ground and struck by a 0.5kg hammer, and (2) a 85 gm weight was actuated by an electrically controlled solenoid. The source was positioned at either end of the geophone bag, offset 0.05m from the adjacent geophones. Four shots were stacked and recorded before moving the system 0.20m along the line and repeating. The other major modification was mounting the seismograph recorder and cables onto a three-wheeled cart so that it could be easily translated along with the sensor array. The seismograph data acquisition and recording system (Geometrics RX-24) was mounted on a jogger/stroller along with the geophone cables and 12 volt automobile battery.

Several steps of data processing were used to convert the raw field data into a seismic reflection image. Seismic traces with the same reflection point (common mid point) were gathered into record sections based on their shot and receiver geometry. The distance between reflection points was 2.5 cm (one-half the receiver spacing), and the number of shot-receiver pairs sharing the same reflection point was typically four. All the traces were filtered for frequencies between 200 and 800 Hz, and normal move-out (NMO) corrected (shifted in time to account for path differences to the same reflection point from different receivers). The data were shifted assuming a velocity of 60 m/s. Muting was applied to the beginning of each trace to eliminate the noise preceding the first arrivals of reflected energy. The traces in each gather were summed (stacked) to enhance reflections while reducing noise. An automatic gain control (AGC) was applied with a time window of 0.015 seconds. AGC results in more uniform data by normalizing the amplitudes within each time window according to the average absolute value of the signal within the window. The resulting traces were migrated in the frequency-wavenumber domain to focus energy at reflecting points (Stolt and Benson, 1986). The conversion from the time-distance domain to the frequency-wavenumber domain used a pad of 30 traces to help minimize edge effects. Frequency-wavenumber migration assumed a constant velocity (60 m/s). Stacking and migration velocities were estimated from a walk-away section (see below), and from individual shot records.

Magnetic Gradiometry

Magnetic surveys are conducted by measuring the earth's magnetic field near the surface of the ground on a grid points. Although the largest contributions to the magnetic field come from the earth's core, differences in the concentration of magnetic materials beneath the surface give rise to variations in the mapped data across the survey grid. In archaeological sites, magnetic differences can result from filled pits or canals, fired or burned earth, or intrusive metal materials (Weymouth, 1986).

Two approaches are used to measure the magnetic field, total field or gradient. In the total field method, the strength of the field is measured. In the gradient method the difference between two sensors, separated by a vertical distance, is measured. The gradient method or magnetic gradiometer reveals near surface features and minimizes the impact of

deeper of large scale features. Using a gradiometer avoids the effect of changing magnetic fields from atmospheric sources, which produce a daily variation with enhanced field strength during local noon.

At the Gila River sites, a Geometrics G858 cesium magnetic gradiometer was operated continuously on grid intervals of 50 cm. The magnetometer had a cycle time of 0.5 sec and a sensitivity of 0.05 nT for each of two sensors, separated by 1 meter in the vertical. The magnetic gradiometer data are processed first by taking the difference between the lower and upper sensors and then by shifting the data backwards along the survey track by 0.3 m to account for delays in sensor recording. An image of the data mapped onto the survey grid show regions of increased magnetic field with white and red colors, and regions with low magnetic field with black and blue colors.

Near Surface Electromagnetic Induction

Electromagnetic induction (EM) uses low frequency electromagnetic waves to detect changes in near surface electrical properties. A transmitting and a receiving coil are separated by a fixed distance, with the coil separation setting the depth penetration for maximum sensitivity. The electromagnetic coupling between the two coils is measured as they are translated along the ground surface. Two properties are derived from the electromagnetic coupling: the electrical conductivity and the magnetic susceptibility, obtained respectively from the out-of-phase and in-phase response. As the coils are moved along the ground surface, changes in the EM signal detect changes in the physical and chemical properties of underlying sediments and soils. Most soil and sediments are poor electrical conductors, and therefore the measurements primarily reveal changes in water saturation, the porosity of the materials, concentration of dissolved electrolytes, the temperature and chemical state of the pore water and the amount and types of clays that are present. Metallic objects also produce strong signatures since they are efficient conductors of electrical energy.

At the Gila River sites, we measured electrical conductivity using the Geonics EM-38, with maximum detection sensitivity at 0.4m depth. Grids of data were collected with measurements taken at 1 m intervals at walking speed along tracks separated by 1m over each survey grid. The data were then gridded for display with white and red colors representing regions of high conductivity, and black and blue colors representing regions of low conductivity

Results

GR-441

The GR-441 site is located in the community of Santan, north of the Gila River, along the piedmont of the Santan Mountains. GPR, MAG and EM were collected along an 18 m (north-south) and 20 m (east-west) grid, and a single line of seismic reflection data were collected in the middle of the survey grid, along an east-west transect (Figure 2). A prehistoric canal was previously documented to run through the survey grid in a northwest-to-southeast direction.

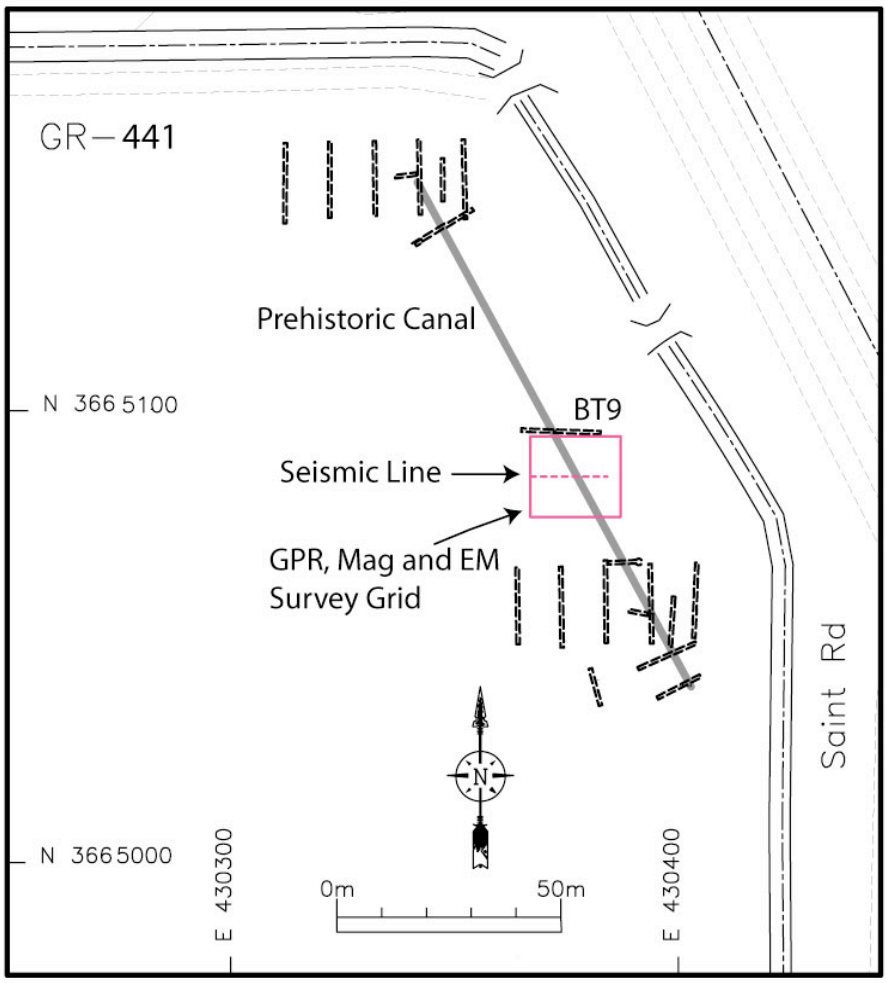

Figure 2. Location of geophysical survey grid (box) and seismic reflection line (dash) at GR-441. Trench BT9 documents a canal (gray line) passing through the grid.

Seismic Reflection Line

To estimate seismic velocity at GR-441, we collected two walk-away record sections, using the hammer (Figure 3a) and solenoid (Figure 3b) sources. From this section, wave velocities were determined based on the range-versus-time slope of coherent events. For each source, shot-receiver offsets were measured from 0 to 6.5 m, consisting of 6 shot points at increasing range, with stationary receivers. Four shots were stacked before successively moving the shot point away from the receivers in 1.25 m steps. Several seismic phases were identified (Figure 3). The air-wave is caused by the sound wave traveling directly to the receivers through the air; it is the first arrival and has a velocity of 343m/s. The air-wave is more prominently produced by the hammer source than the solenoid. The P-wave arrives later, having traveled at about 90m/s; these are produced with higher amplitude by the hammer source, but are also well resolved with the solenoid source at the maximum range. Surface waves, also called “ground-roll”, travel slower, with velocities of about 60m/s and are seen with both sources.

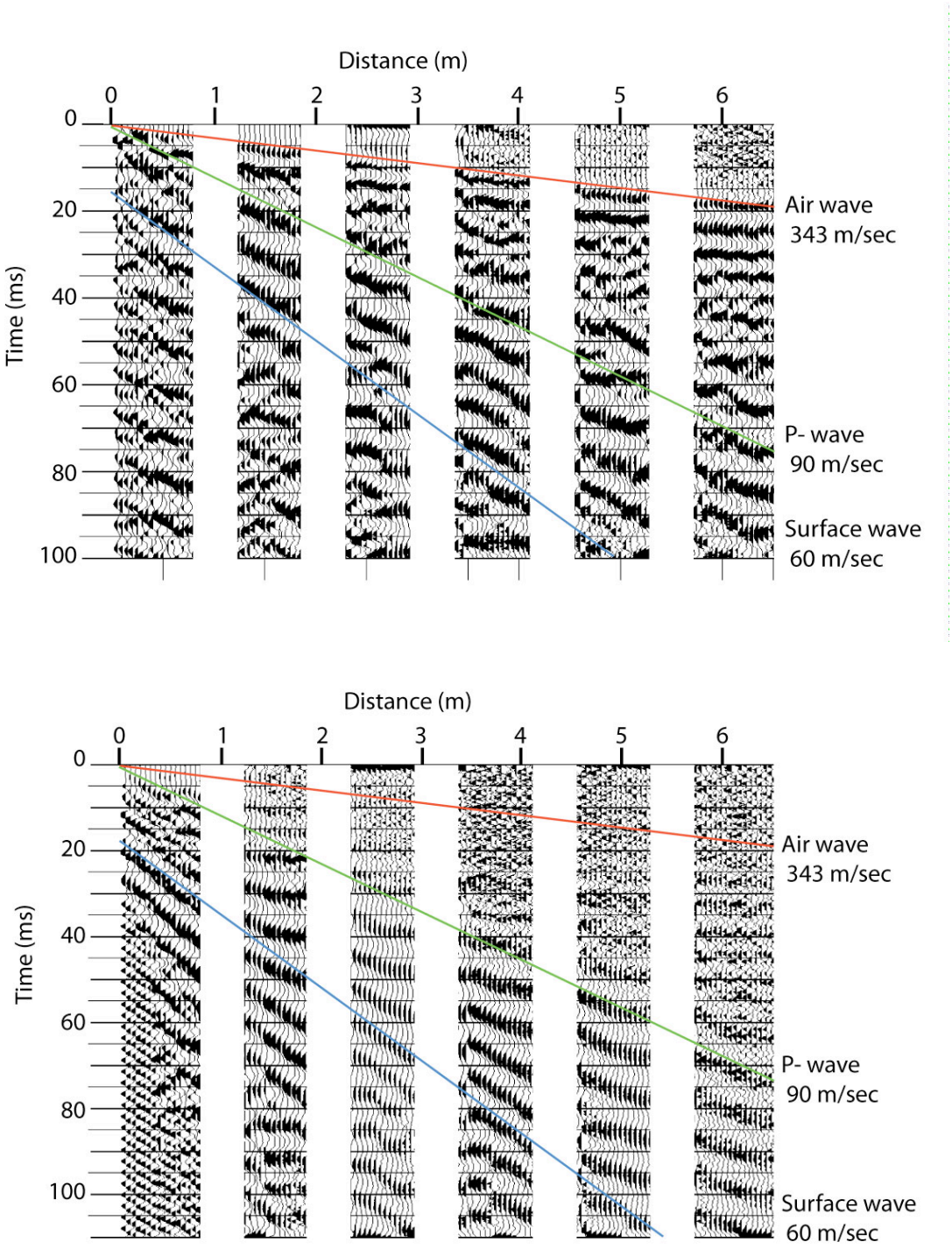

Figure 3. Record section of seismic waves at GR441 using hammer (upper panel) and solenoid source (lower panel). Indicated waves include: air-wave (343 m/sec), P-wave (90 m/sec) and surface wave (60 m/sec).

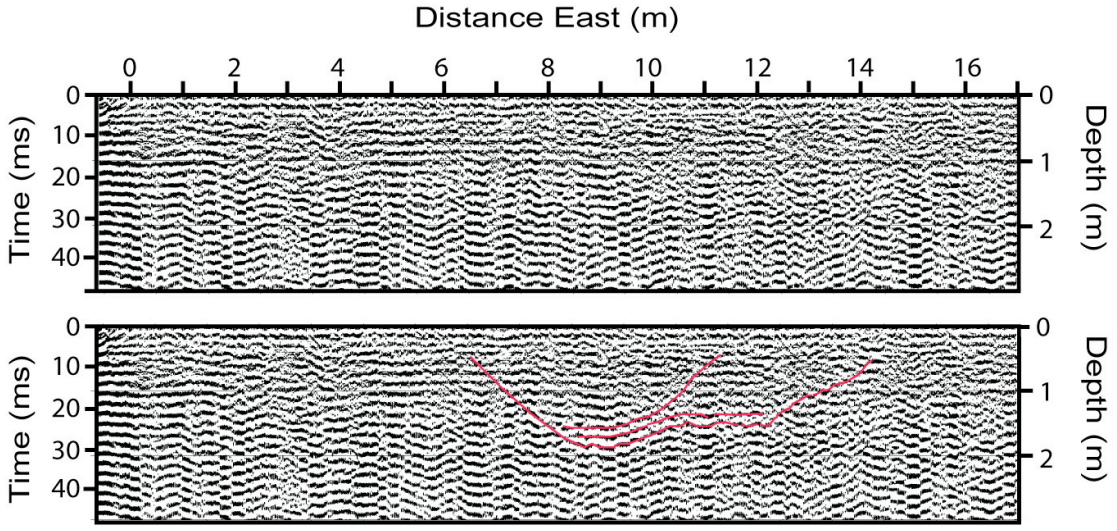

Figure 4. Seismic reflection image from GR-441 using the hammer source. Lower panel has added annotation (red) of concave reflecting event, presumed to be from the canal.

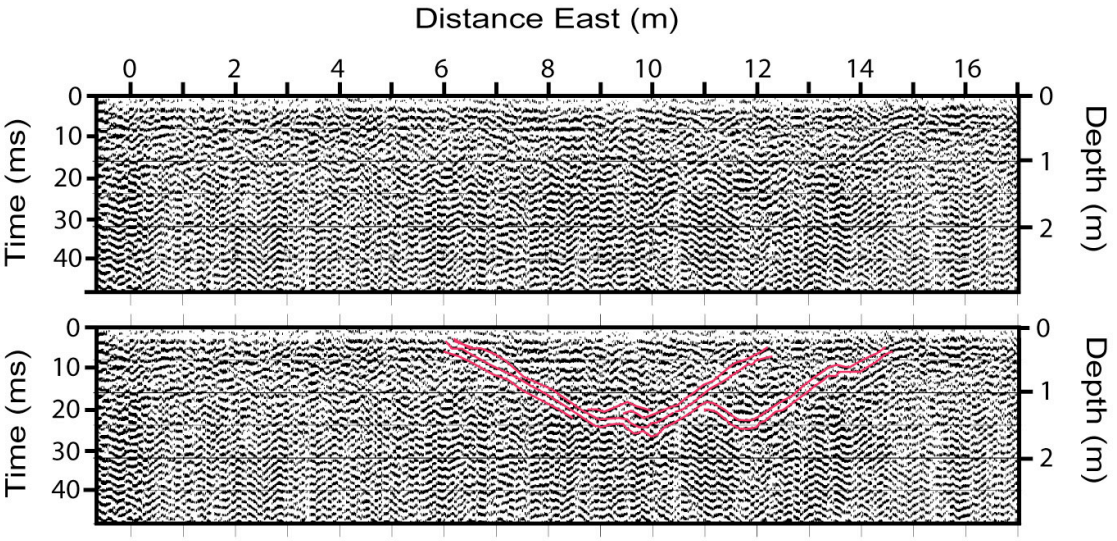

Figure 5. Seismic reflection image from GR-441 using the solenoid source. Lower panel has added annotation (red) presumed to be from the canal.

A single line of seismic reflection data were collected at the GR-441 site (Figure 4). At each shot-point, the hammer source and the solenoid source were used sequentially, so that the data were collected alternately, and the geophones were only moved along the line for a single passage. The line was about 20 m long and was completed in about 4 hours of field time. Site conditions were extremely hot and dry (> 100 °F) at the time of the survey.

The seismic image resulting from the hammer source is shown in Figure 5. The upper panel shows the image as a series of trace amplitudes with time along the left side of the plot and presumed depth along the right side. In the middle of the image, from range = 6 – 14 meters, a concave reflector is observed, with a maximum depth of about 1.9 m at 9 m range. The lower panel shows an annotated image, with the outline of the concave reflector illuminated in red. This reflector has the same position and depth as the prehistoric canal. A similar concave reflection is observed in the seismic image resulting from the solenoid (Figure 5), and a second set of sloping reflectors are seen on the east side of the main concave reflector in the solenoid image. Despite similar data processing steps being applied to both the hammer and the solenoid source, the solenoid has somewhat higher seismic frequency content (550 Hz peak energy) relative to the hammer (400 Hz peak energy).

The concave reflecting layers of Figure 4 and 5 are presumed to result from reflection contrasts between the silty loam surrounding the canal, and the silt and clay deposits which make up the fill and the floor of the canal (Figure 6).

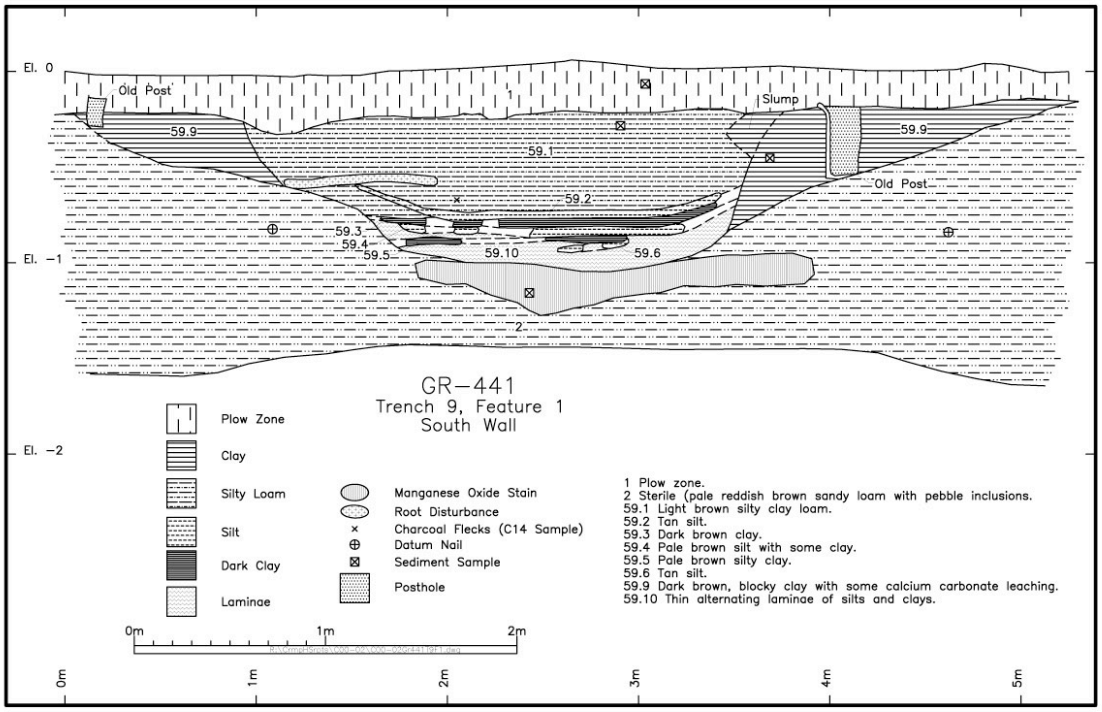

Figure 6. Stratigraphy of the canal at GR-441 from trench 9.

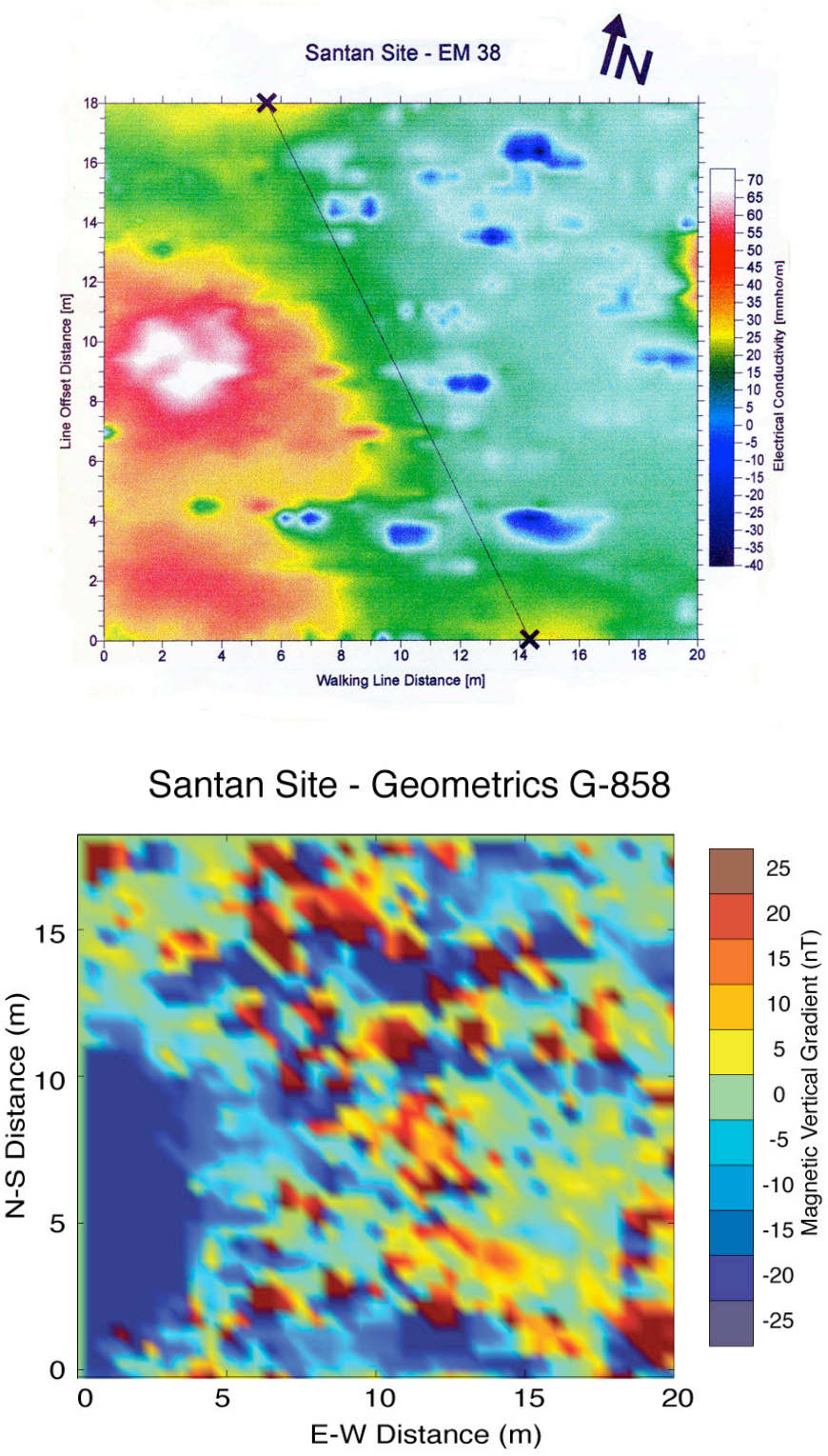

Figure 7. Electrical conductivity (upper panel) and magnetic vertical gradient (upper panel) at GR-441. The location of the canal center is shown as a black line on upper panel.

EM and MAG Survey Grid

The EM and MAG survey grid at GR-441 are located south of backhoe trench 9 (Figure 2); the prehistoric canal passes through the center of the survey grid in a northwest-southeast trending direction.

Electrical conductivity measured by the EM-38 (Figure 7) show generally higher conductivity in the western side of the grid, as well as several point sources of low conductivity in the eastern side of the grid. Magnetic vertical gradient data (Figure 7) also reflect a smoother pattern with low field strength in the western portion of the grid, and a collection of high point sources of field in the eastern portion of the grid. Taken together the EM and MAG data suggest that the grid is contaminated by modern metal debris, which produce point sources of high conductivity and magnetic field in the eastern portion of the grid. In the absence of metal debris, note that the conductivity trends in the western portion of the grid follow the general direction of the canal.

GR-1086

The GR-1086 site is located adjacent to Crown Road, north of the Gila River (Figure 1). GPR, MAG and EM were collected along a northeast-southwest trending grid of dimensions 20 m x 5 m (Figure 8). A prehistoric canal, previously revealed by backhoe trench 97, traverses the site in an east-west direction and bisects the long axis of the survey grid at an oblique angle. The canal stratigraphy seen in BT 97 is shown in Figure 9.

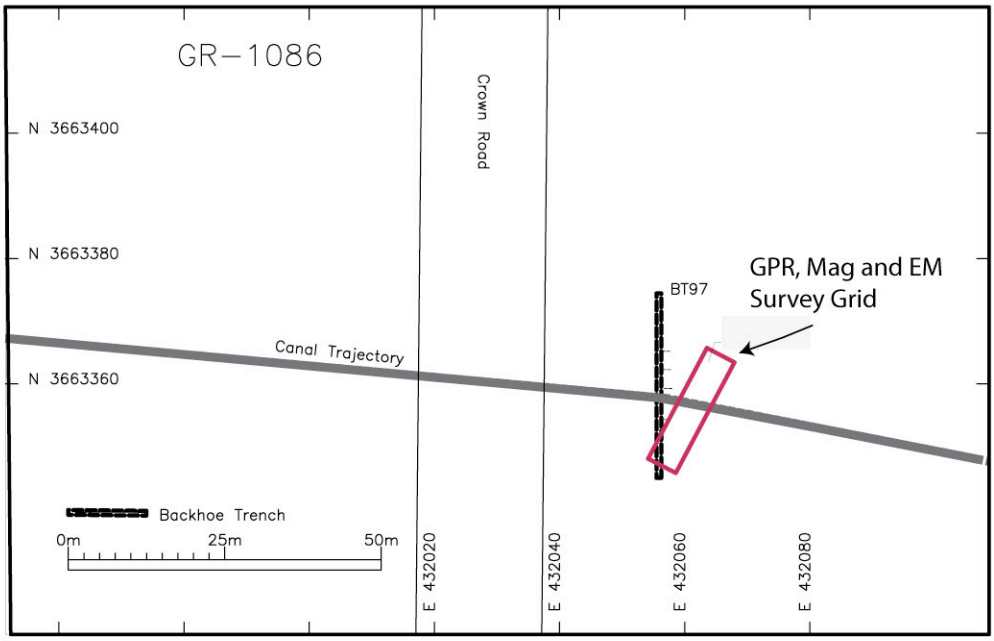

Figure 8. Location of geophysical survey grid (box) at GR-1086. Backhoe trench BT97 documents a canal (gray line) passing through the grid.

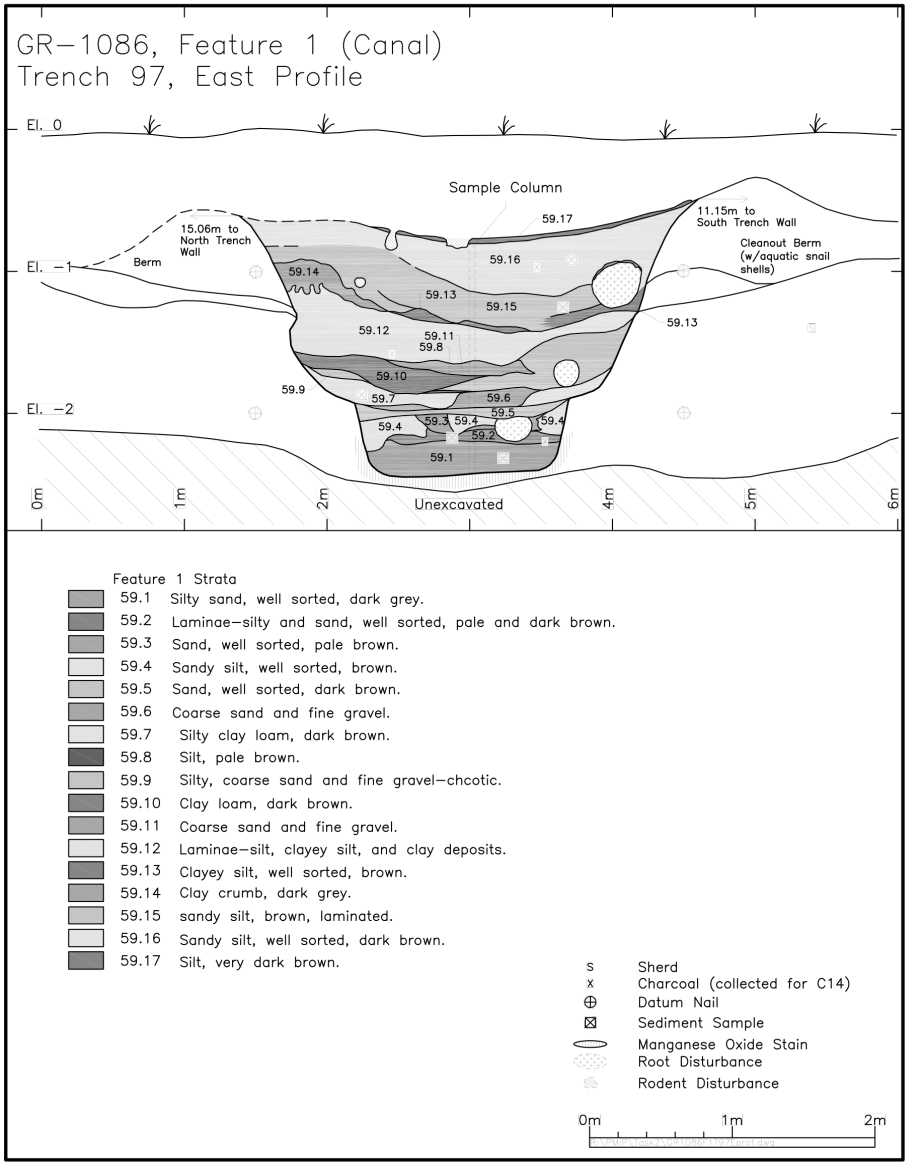

Figure 9. Stratigraphy of the canal at GR-1086 from trench BT97.

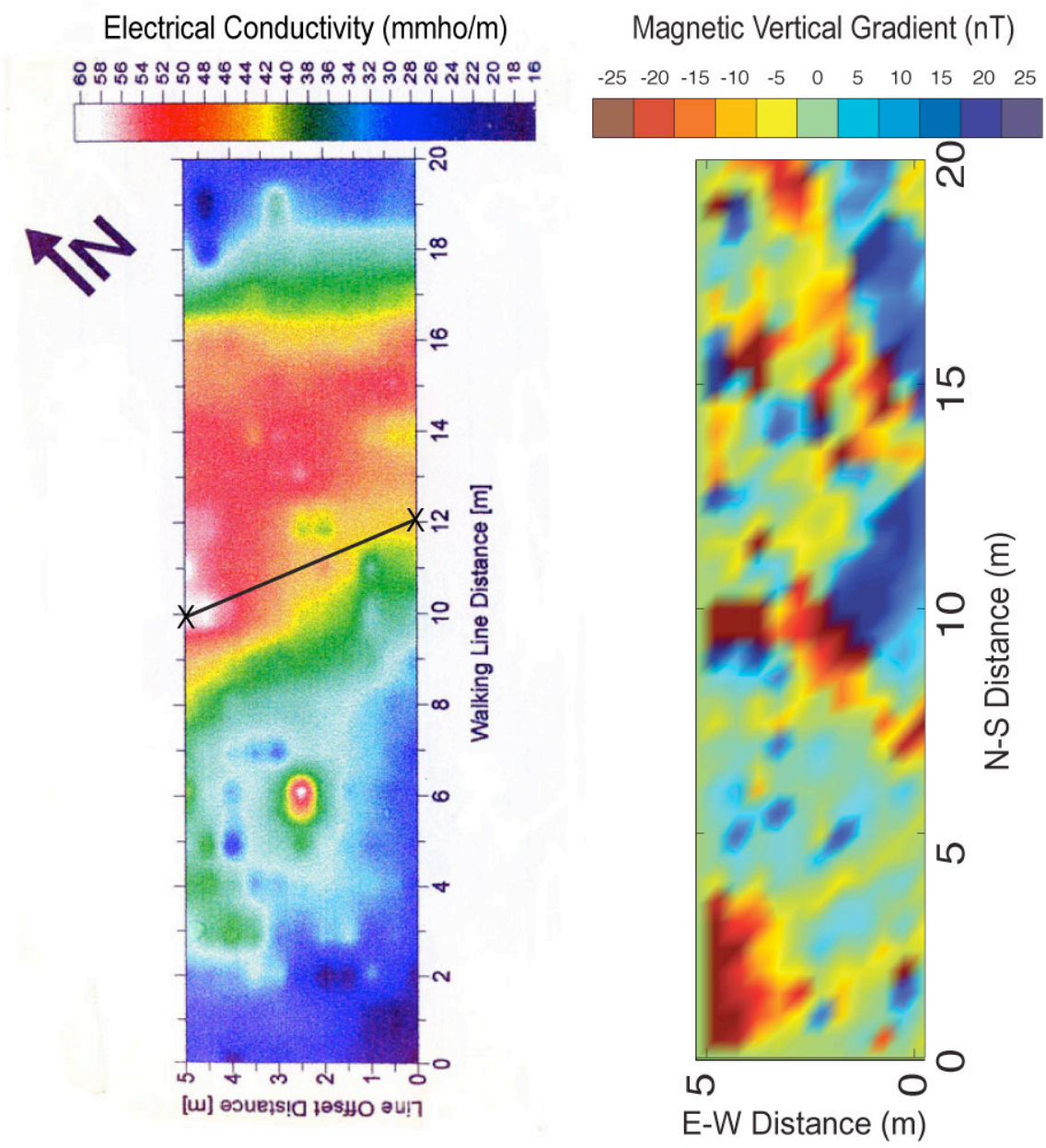

Figure 10. Electrical conductivity (left panel) and magnetic vertical gradient (right panel) at GR-1086. The location of the canal center is shown as a black line in left panel.

EM and MAG Survey Grid

The EM and MAG surveys at GR-1086 were conducted on a grid to the east of backhoe trench 97 (Figure 8); a prehistoric canal passes through the center of the survey grid in an approximately east-west trending direction. Electrical conductivity measurements at GR-1086 reveal a band of high conductivity in the northern portion of the grid (Figure 10). The dividing line between high and low conductivity area is roughly coincident with the approximate location of the canal (black line in Figure 10). Magnetic vertical gradient data

reveal many point sources distributed throughout the grid (Figure 10). In addition, a broader region of low field strength is seen on the eastern edge of the grid.

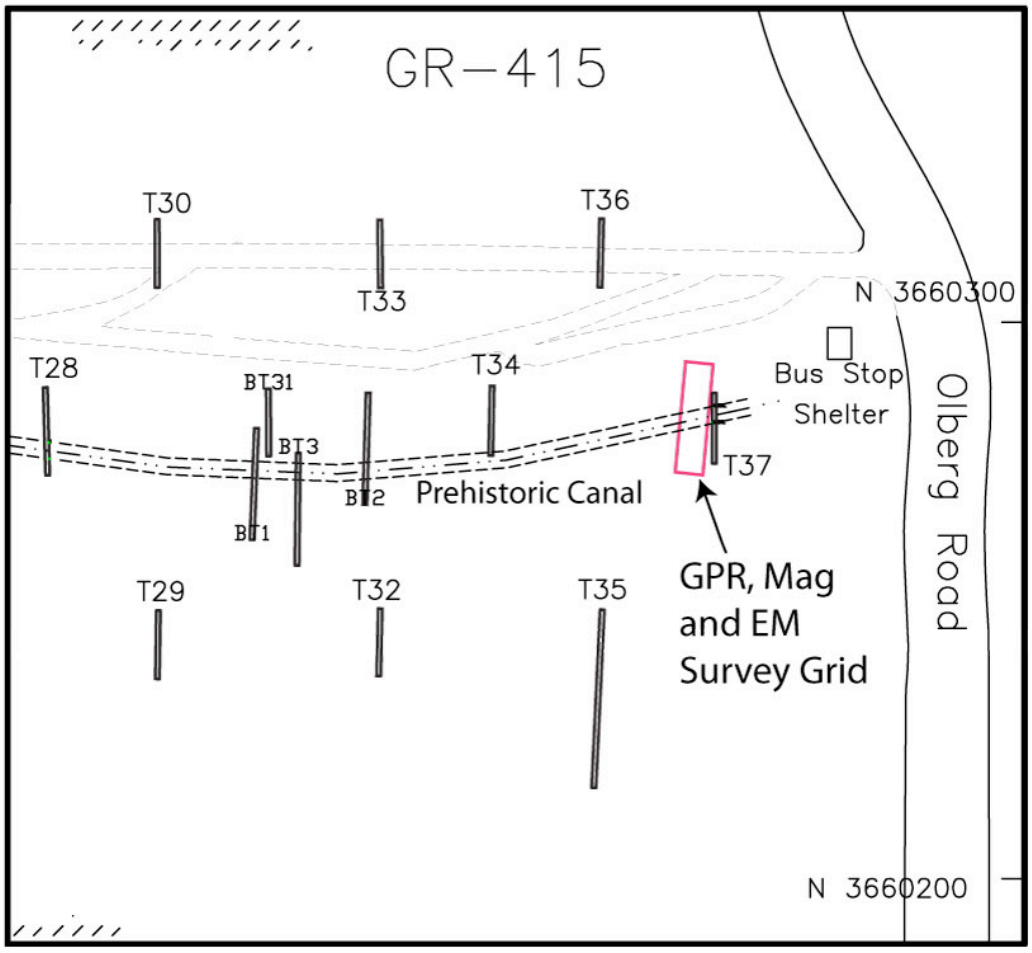

Figure 11. Location of geophysical survey grid (box) at GR-415. Several trenches document a canal (dashed lines) passing through the grid in an east-west direction.

GR-415

The GR-415 site is located adjacent to Olberg Road, south of Gila River (Figure 1). GPR, MAG and EM were collected along a northeast-southwest trending grid of dimensions 20 m x 5 m (Figure 11). A prehistoric canal, previously revealed by several trenches, traverses the site in an east-west direction and bisects the long axis of the survey grid at an oblique angle (Figure 11). The canal stratigraphy, documented in T28 west of the survey grid, is shown in Figure 12.

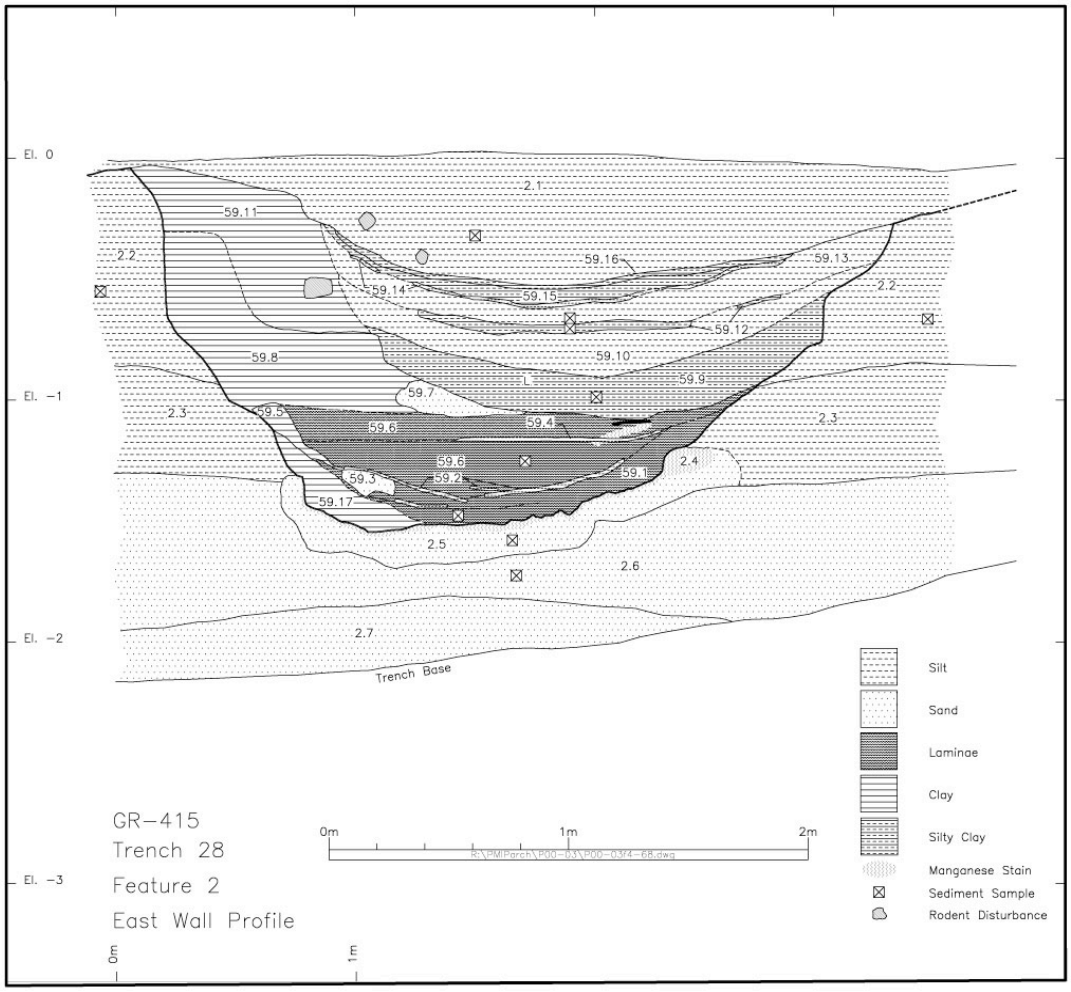

Figure 12. Stratigraphy of the canal at GR-415 from trench T28.

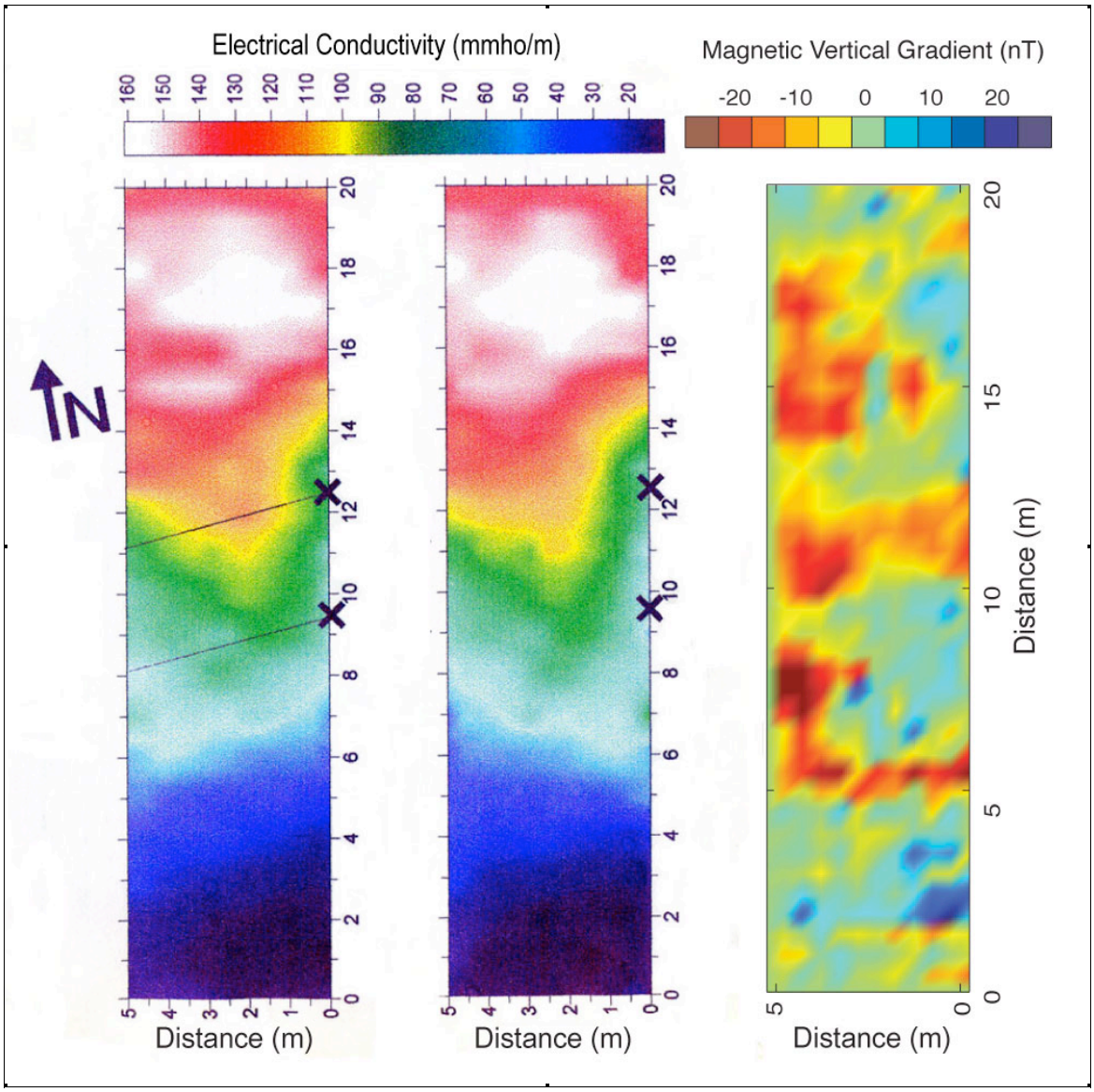

Figure 13. Electrical conductivity walking north-south (left panel) and east-west (center panel) and magnetic vertical gradient (right panel) at GR-415. Locations of the canal margins are shown as black lines in the left panel.

EM and MAG Survey Grid

The EM and MAG surveys at GR-415 were conducted on a grid to the west of trench 37 (Figure 11); a prehistoric canal passes through the survey grid in an approximately east-west trending direction. Electrical conductivity measurements at GR-415 were collected by walking in the north-south direction (Figure 13 left panel), as well as by walking in the east-west direction (Figure 13 center panel). These two EM images are quite similar in overall appearance; they both suggest a region of high conductivity in the northern portion of the grid, approximately corresponding to the northern margin of the

canal. The magnetic vertical gradient data reveal broad regions of high field strength on the western edge of the grid.

Discussion

Key processes that formed the Gila River canal deposits are hydraulic sediment transport and mineral deposition. Following abandonment, aeolian processes resulted in canal in-filling and plowing resulted in disturbance of the surface layer. Trench 9 at GR-441 (Figure 6) illustrates the canal stratigraphy with clay deposits forming the walls and bottom of the canal, and silty-loam filling the interior. Beneath the canal bottom is a zone of manganese oxide stain, most likely mineral deposits from evaporation.

Seismic reflection images of the canal at GR-441 that generally follow the expected features of the canal as revealed in a nearby cross-section (trench 9). Both the hammer and solenoid source display a concave reflector whose bottom is at 1.5 m depth and whose sides slope at 25-30 degrees. Both images also suggest a potential second margin of the canal, about 2 meters to the east, perhaps remnant of an earlier canal. The solenoid source does a better job of defining the canal, perhaps related to its higher frequency content than the hammer source (550 Hz energy for solenoid versus 400 Hz for hammer). The reflections seen in the seismic images are potentially due to an impedance contrast between the clays and manganese oxide deposit that make up the sides and walls of the canal, relative to the less consolidated silty-loam fill.

The electrical conductivity for each of the three Gila River sites showed broad regions of high and low conductance, roughly correlated with the location of the buried canals. Clay materials are known to impact the electrical conductivity of soils (McNeill 1980) and we presume that the regions of high conductivity may be related to clay content associated with the canals, although there may be additional factors impacting these measurements.

Magnetic vertical gradiometer measurements were contaminated by modern metal present on these sites, leaving it an open question whether this technique would be able to map the buried Gila River canals in the absence of these high amplitude interfering sources. Ground penetrating radar at 400 MHz was not able to image the buried canals owing to high signal attenuation and therefore small depth of penetration.

Acknowledgements

Project support was provided by the Gila River Indian Community. We thank John Ravesloot, Bob Neely and Mike Foster and for help in the field and logistical support. We thank David Wright for encouragement and support to complete data analysis and reporting.

References

Conyers, L. B. (2004). Ground-penetrating Radar for Archaeology. AltaMira Press, Walnut Creek, California.

Conyers, L. B. and J. E. Lucius (1996) Velocity analysis in archaeological ground-penetrating radar studies, Archaeological Prospection 3: 25-38.

Hildebrand, J.A., Wiggins, S.M., Henkart, P.C., & Conyers, L.B. (2002). Comparison of seismic reflection and ground-penetrating padar imaging at the controlled archaeological test site, Champaign, Illinois. Archaeological Prospection, 9: 9-21.

Hildebrand, J. A., S. M. Wiggins, J. L. Driver, and M. R. Waters. (2007). Rapid seismic reflection imaging at the Clovis period Gault site in central Texas. Archaeological Prospection 14: 245-260.

Jones, R. E., Isserlin, B. S. J., Karastathis, V., Paramarinopoulos, S. P., Syrides, G. E., Uren, J., Balatsas, I., Kapopoulos, C., Maniatis, Y. and Facorellis, G. (2000). Exploration of the Canal of Xerxes, Northern Greece: the role of geophysical and other techniques. Archaeological Prospection, 7: 147–170.

Karastathis, V. K., S. Papamarinopoulos, and R. E. Jones, (2001). 2-D velocity structure of the buried ancient canal of Xerxes: an application of seismic methods in archaeology, Journal of Applied Geophysics 47: 29-43.

SIOSEIS. (2010). (Version 2010.3.3) [Computer software]. San Diego, CA: National Science Foundation (NSF) and Scripps Industrial Associates. (http://sioseis.ucsd.edu/)

Steeples, D.W., Baker, G.S., Schmeissner, C., & Macy, B.K. (1999). Geophones on a board. Geophysics, 64, 809-814.

Stolt, R.H. & Benson, A.K. (1986). Seismic migration: Theory and practice. London: Geophysical Press Ltd.

Waters, M. R. and J. C. Ravesloot (2000) Late Quaternary Geology of the Middle Gila River, Gila River Indian Reservation, Arizona, Quaternary Research, Volume 54: 49-57.

Weymouth, J. W. (1986) Archaeological site surveying program at the University of Nebraska. Geophysics 51, 538-552.